Pitch Stability Analysis
for Mechanical-Hydraulic-Structural-Fluid
Coupling System of High-Lift Hoist Vertical Shiplift

Yang Zhang[1,2] – Duanwei Shi[1,2,*] – Tong Xiao[2] – Ji Zhou[2] – Xionghao Cheng[2]

[1]Wuhan University, Key Laboratory of Hydraulic Machinery Transients, China
[2]Wuhan University, School of Power and Mechanical Engineering, China

Pitch stability of the high-lift wire rope hoist vertical shiplift under dynamic hydraulic levelling has always been an issue of concern. It not only affects working efficiency but also brings significant challenges to operational safety. A new mechanical-hydraulic-structural-fluid (MHSF) coupling dynamics model and a developed semi-analytical method are presented for stable property analysis. The models of the hydraulic levelling subsystem, shallow water sloshing subsystem, the main hoist mechanical subsystem, and the shiplift chamber structure subsystem are built using a closed-loop transfer function, multi-modal theory, and an second-type Lagrangian equation, respectively. Then, a core twenty-one order state matrix of the MHSF coupling system is established using the state-space method. Subsequently, the Lyapunov motion stability theory and Eigen-analysis method are used in combination to judge the pitch stability and analyse the characteristics of the subsystems. Taking four typical high-lift hoist vertical shiplifts as examples, the rationality of the proposed model and method is validated. The results indicate that although the pitch stability safety factor under hydraulic dynamic levelling is reduced by about 15 % to 44 % with respect to hydraulic static levelling, hydraulic dynamic levelling still can meet stability requirements. Furthermore, for the designed 200 m level hoist vertical shiplift, the preliminary design parameters can ensure the pitch stability safety factor under dynamic hydraulic levelling of not less than 1.1. The element most prone to instability is the shallow water sloshing subsystem; increasing the synchronous shaft stiffness or the water boundary layer damping ratio can effectively enhance the pitch stability.
Keywords: shiplift, pitch stability, hydraulic levelling, Eigen-analysis, dynamics

Highlights
- *A new mechanical-hydraulic-structural-fluid (MHSF) coupling dynamics model of high-lift hoist vertical shiplift has been established.*
- *A developed semi-analytical method has been presented to analyse the pitch stability characteristics.*
- *Pitch stability under hydraulic dynamic levelling is reduced by 15 % to 44 % with respect to hydraulic static levelling, but hydraulic dynamic levelling will not cause instability.*
- *For the designed 200 m level shiplift, improving the synchronous shaft stiffness by 30 % can enhance the pitch stability by about 6.2 %; doubling the water boundary layer damping ratio can raise the pitch stability about 20.57 %.*

0 INTRODUCTION

As a core component in a large hydropower station, the high-lift hoist vertical shiplift is pre-developed in China. It uses cables to raise the ship to overcome the water level difference between upstream and downstream. Since the lift height of the 200 m level hoist vertical shiplift (abbreviated as 200 m level shiplift) is nearly double that of the Three Gorges shiplift, the pitch stability problem becomes more complicated. For the vast majority of hoist vertical shiplifts, a hydraulic levelling subsystem has been set up, for levelling the shiplift chamber and balancing the tension of cables. However, once the hydraulic levelling subsystem is started during operation (dynamic hydraulic levelling), it will form a complex mechanical-hydraulic-structural-fluid (MHSF) coupling system. Its dynamic stability and the ability to resist the overturning are not apparent,

so only starting the hydraulic levelling subsystem after stopping the shiplift (hydraulic static levelling) is allowed at present [1] and [2]. In order to ensure operational safety and avoid unnecessary downtime, pitch stability under dynamic hydraulic levelling should be studied in depth.

Previous research studies on the shiplift system model are incomplete. The ship-water-chamber coupling motion equations are established to analyse the time response [3]. However, the primary hoist subsystem is ignored, which plays an essential role in ensuring pitch stability. Liao [4] and Cheng et al. [5] built a coupling dynamics model of main hoist subsystem, shiplift chamber, and sloshing, but neglected the torque counterweight in the main hoist subsystem; the latter is an essential part in the fully balanced quality system. A nine-degree-of-freedom (DOF) model of the primary hoist subsystem (including hoist, pulley, wire rope,

*Corr. Author's Address: School of Power and Mechanical Engineering, Wuhan University, Wuhan, China, dwshi@whu.edu.cn

torque counterweight, gravity counterweight, and synchronous shaft), shiplift chamber, and shallow water sloshing was developed by Zhang et al. [6]. The pitch stability problem under hydraulic static levelling can be solved very well, but the hydraulic levelling subsystem remains ignored; it is important to balance and equalize the tension between the wire ropes and adjust the level of shiplift chamber. In the newly proposed MHSF coupling dynamics model, the main hoist subsystem, shiplift chamber subsystem, hydraulic levelling subsystem, and shallow water sloshing subsystem will be considered completely to analyse the pitch stability under hydraulic dynamic levelling. This is a critical issue for current shiplift designers and researchers.

For the relatively simple mechanical [7] and [8] and mechanical-fluid [9] system, the Lyapunov function is commonly used to judge the stability. However, it is difficult to construct the Lyapunov function directly from the complex shiplift system. The convergence of the time-domain response is focused on analysing the complex hydraulic-mechanical-electrical-structural system [10]. However, for the MHSF coupling system with a large difference in response frequency, it is too easy to form ill-conditioned equations. The hydraulic levelling subsystem is treated as a first-order system, and the tension equalization characteristics and dynamic system responses are analysed [11]. It is a good attempt, but the simplification of the hydraulic levelling subsystem and the lack of shallow water sloshing subsystems are inappropriate for pitch stability analysis. The Routh-Hurwitz theory [12] and [13] and Lyapunov motion stability theory [14] and [15] have been proved to rate the stability effectively. However, its analysis of the intrinsic connection of the coupling system is powerless. Eigen-analysis and the state-space method are adopted to investigate the stability of the hydraulic-mechanical-electrical coupling mechanism of a hydropower plant [16] to [19].

In the present study, a new MHSF coupling dynamics model for high-lift hoist vertical shiplift will be established. Furthermore, a developed semi-analytical method integrating the Lyapunov motion stability theory and Eigen-analysis will be proposed to judge the pitch stability and analyse the internal connection of the coupling system under dynamic hydraulic levelling. Four typical high-lift hoist vertical shiplifts will be taken as examples to validate the proposed model and method. The subsystem stability priority will be interpreted. In addition, the influence of lift height, synchronous shaft stiffness and subsystem damping ratio on the pitch stability will be researched in detail.

1 METHODS

In the process of ascension, the shiplift chamber suspended by cable is inevitably pitched due to the manufacturing error of the hoist diameter, the wire rope diameter and elastic modulus [20]. As shown in Fig. 1, the shiplift chamber is subjected to pitch motion during operation, and the clamping equipment, the safety brake, and the working brake have been released.
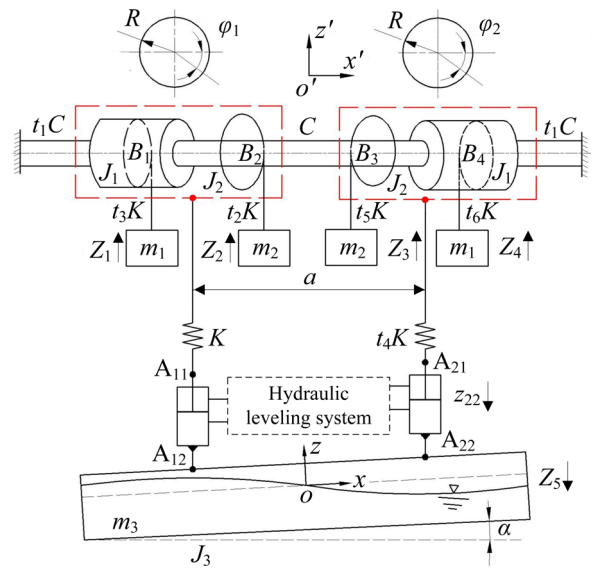
Fig. 1. A 10DOF (φ_1, φ_2, α, Z_1, Z_2, Z_3, Z_4, Z_5, z_{22}, β_1) MHSF coupling dynamics model of high-lift hoist vertical shiplift

A new MHSF coupling system is established under the earth-fixed coordinate system ($o'x'z'$). In order to illustrate the mathematical model, the coupling system is decoupled as the main hoist mechanical subsystem, hydraulic levelling subsystem, rigid shiplift chamber structure subsystem and shallow water sloshing subsystem. The main hoist mechanical subsystem is a mechanical device that suspends the chamber and drives it up and down; it mainly consists of the hoist lift mechanism (B_1, B_2, B_3, B_4), synchronous shaft (C, t_1C), counterweight (m_1, m_2) and wire rope (K, t_4K, t_2K, t_3K, t_5K, t_6K).

1.1 Shallow Water Sloshing Subsystem Model

The shiplift chamber is a typical rectangular water container with low filling depth ratio ($H/L < 0.05$).

Since the variation range of water along the length distribution is much larger than that along the width distribution, a two-dimensional rigid shiplift chamber with a unitary width is adopted [21], as shown in Fig. 2. oxz is the shiplift chamber-fixed coordinate system located at the centre of the mean free surface (Σ_0).
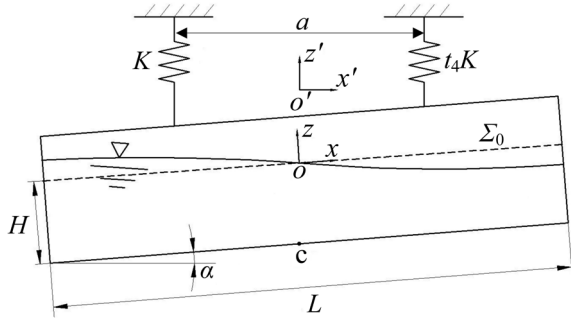
Fig. 2. *Shallow water sloshing in the shiplift chamber under pitch motion*

Previous research [22] has shown that the peak hydrodynamic moment reaches maximum value under pure pitch motion instead of coupled vertical and pitch motions. To ensure the safety, pure pitch motion (more dangerous) will be further investigated. According to the studies of [6] and [23], the modal system of shallow water sloshing and hydrodynamic moment can be written as:

$$\ddot{\beta}_1 + 2\xi_w \omega_1 \dot{\beta}_1 + \omega_1^2 \beta_1 = \frac{4Hg}{L}\alpha + \frac{4H^2}{L}\ddot{\alpha}, \quad (1)$$

$$M = -\frac{3}{2500}\rho BHL^3\ddot{\alpha} + \frac{2L}{\pi^4 H^2}\rho BHL^3\ddot{\beta}_1. \quad (2)$$

1.2 Hydraulic Levelling Subsystem Model

The hydraulic levelling subsystem consists of levelling hydraulic cylinders and a hydraulic control system. If the situation of Fig. 1 appears, the control strategy is keeping the state of A_{11} point unchanged, and controlling the A_{21} point to approach A_{11} through the hydraulic system. The modelling of the hydraulic levelling subsystem mainly includes the proportional
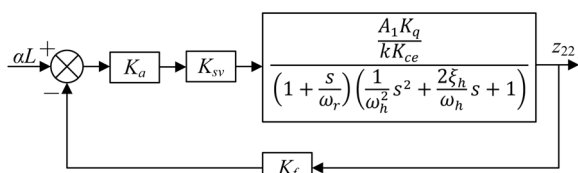
Fig. 3. *Closed-loop transfer function block diagram of hydraulic levelling system*

amplifier, the proportional speed regulating valve, valve controlled asymmetric hydraulic cylinder, and shiplift chamber level sensor. Because of the working frequency of proportional amplifiers, the proportional speed regulating valve and shiplift chamber level sensor is much higher than that of the hydraulic cylinder, so these are linearized into proportional links.

As shown in Fig. 3, according to the linear flow equation, the flow continuity equation and force balance equation [24], the transfer function of the valve controlled asymmetric hydraulic cylinder $G(s)$ can be derived as:

$$G(s) = \frac{\dfrac{A_1 K_q}{kK_{ce}}}{\left(1 + \dfrac{s}{\omega_r}\right)\left(\dfrac{s^2}{\omega_h^2} + \dfrac{2\xi_h}{\omega_h}s + 1\right)}, \quad (3a)$$

$$\omega_h = \sqrt{\left[\frac{2(1+n^2)\beta_e A_1^2}{M_t V_t} + \frac{k}{M_t}\right]}, \quad (3b)$$

$$\xi_h = \frac{\dfrac{K_{ce}}{2A_1}\sqrt{\dfrac{2(1+n^2)\beta_e M_t}{V_t}}}{\left[1 + \dfrac{kV_t}{2(1+n^2)\beta_e A_1^2}\right]^{\frac{3}{2}}}, \quad (3c)$$

$$\omega_r = \frac{K_{ce}}{A_1^2\left[\dfrac{1}{k} + \dfrac{V_t}{2(1+n^2)\beta_e A_1^2}\right]}, \quad (3d)$$

here $n = A_2/A_1$, $K_{ce} = K_c + C_t$ and $k = t_4 K$.

According to Fig. 3, the closed-loop transfer function of the hydraulic levelling subsystem $G_B(s)$ is as follows:

$$G_B(s) = \frac{\dfrac{A_1 K_q}{kK_{ce}}K_a K_{sv}\omega_r\omega_h^2}{\left[\begin{array}{c}s^3 + (2\xi_h\omega_h + \omega_r)s^2 + (\omega_h^2 + 2\xi_h\omega_r\omega_h)s + \\ +(1 + \dfrac{A_1 K_q}{kK_{ce}}K_a K_{sv}K_f)\omega_r\omega_h^2\end{array}\right]}. \quad (4)$$

The input of the hydraulic levelling system is the displacement deviation of the shiplift chamber (αL), and the output is the piston displacement (z_{22}). Thus, the dynamic model can be derived based on Eq. (4).

$$\dddot{z}_{22} + (2\xi_h\omega_h + \omega_r)\ddot{z}_{22} + (\omega_h^2 + 2\xi_h\omega_r\omega_h)\dot{z}_{22} + $$
$$+ \left(1 + \frac{A_1 K_q}{kK_{ce}}K_a K_{sv}K_f\right)\omega_r\omega_h^2 z_{22} - \quad (5)$$

$$-\frac{A_1 K_q}{k K_{ce}} K_a K_{sv} \omega_r \omega_h^2 L\alpha = 0. \qquad \text{cont.(5)}$$

1.3 Main Hoist Mechanical Subsystem Model

The kinetic energy and potential energy of the main hoist mechanical and shiplift chamber structure subsystem can be defined as:

$$T = \frac{1}{2}J_1\left(\dot{\varphi}_1^2 + \dot{\varphi}_2^2\right) + \frac{1}{2}J_2\left(\dot{\varphi}_1^2 + \dot{\varphi}_2^2\right) + \frac{1}{2}J_3\dot{\alpha}^2 +$$
$$+\frac{1}{2}m_1\dot{Z}_1^2 + \frac{1}{2}m_2\dot{Z}_2^2 + \frac{1}{2}m_2\dot{Z}_3^2 + \frac{1}{2}m_1\dot{Z}_4^2 + \frac{1}{2}m_3\dot{Z}_5^2, \qquad (6)$$

$$V = \frac{1}{2}K\left(R\varphi_1 - Z_5 - \frac{1}{2}a\alpha\right)^2 +$$
$$+\frac{1}{2}t_4K\left(R\varphi_2 - z_{22} - Z_5 + \frac{1}{2}a\alpha\right)^2 + \frac{1}{2}t_3K\left(R\varphi_1 + Z_1\right)^2 +$$
$$+\frac{1}{2}t_2K\left(R\varphi_1 + Z_2\right)^2 + \frac{1}{2}t_5K\left(R\varphi_2 + Z_3\right)^2 +$$
$$+\frac{1}{2}t_6K\left(R\varphi_2 + Z_4\right)^2 + \frac{1}{2}C\left(\varphi_1 - \varphi_2\right)^2 + \frac{1}{2}t_1C\left(\varphi_1^2 + \varphi_2^2\right). (7)$$

Considering the torsional vibration damping ratio ξ_j and wire rope damping ratio ξ_g, the dynamic model of the primary hoist mechanical subsystem can be derived using the second type Lagrangian equation.

$$\ddot{\varphi}_1 + 2\xi_j\sqrt{\frac{\left(C + t_2KR^2 + t_3KR^2 + t_1C + KR^2\right)}{\left(J_1 + J_2\right)}}\dot{\varphi}_1 +$$
$$+\frac{\left(C + t_2KR^2 + t_3KR^2 + t_1C + KR^2\right)}{\left(J_1 + J_2\right)}\varphi_1 -$$
$$-\frac{KR}{\left(J_1 + J_2\right)}Z_5 - \frac{aKR}{2\left(J_1 + J_2\right)}\alpha + \frac{t_3KR}{\left(J_1 + J_2\right)}Z_1 +$$
$$+\frac{t_2KR}{\left(J_1 + J_2\right)}Z_2 - \frac{C}{\left(J_1 + J_2\right)}\varphi_2 = 0, \qquad (8)$$

$$\ddot{\varphi}_2 + 2\xi_j\sqrt{\frac{\left(t_6KR^2 + t_5KR^2 + C + t_1C + t_4KR^2\right)}{\left(J_1 + J_2\right)}}\dot{\varphi}_2 +$$
$$+\frac{\left(t_6KR^2 + t_5KR^2 + C + t_1C + t_4KR^2\right)}{\left(J_1 + J_2\right)}\varphi_2 -$$
$$-\frac{t_4KR}{\left(J_1 + J_2\right)}z_{22} - \frac{t_4KR}{\left(J_1 + J_2\right)}Z_5 + \frac{t_4aKR}{2\left(J_1 + J_2\right)}\alpha +$$
$$+\frac{t_5KR}{\left(J_1 + J_2\right)}Z_3 + \frac{t_6KR}{\left(J_1 + J_2\right)}Z_4 - \frac{C}{\left(J_1 + J_2\right)}\varphi_1 = 0, \qquad (9)$$

$$\ddot{Z}_1 + 2\xi_g\sqrt{\frac{t_3K}{m_1}}\dot{Z}_1 + \frac{t_3K}{m_1}Z_1 + \frac{t_3KR}{m_1}\varphi_1 = 0, \qquad (10)$$

$$\ddot{Z}_2 + 2\xi_g\sqrt{\frac{t_2K}{m_2}}\dot{Z}_2 + \frac{t_2K}{m_2}Z_2 + \frac{t_2KR}{m_2}\varphi_1 = 0, \qquad (11)$$

$$\ddot{Z}_3 + 2\xi_g\sqrt{\frac{t_5K}{m_2}}\dot{Z}_3 + \frac{t_5K}{m_2}Z_3 + \frac{t_5KR}{m_2}\varphi_2 = 0, \qquad (12)$$

$$\ddot{Z}_4 + 2\xi_g\sqrt{\frac{t_6K}{m_1}}\dot{Z}_4 + \frac{t_6K}{m_1}Z_4 + \frac{t_6KR}{m_1}\varphi_2 = 0. \qquad (13)$$

1.4 Shiplift Chamber Structure Subsystem Model

The rigid shiplift chamber is subjected to pitch and vertical motions during operation. Considering the pitch motion damping ratio ξ_p and vertical motion damping ratio ξ_v, the model of the shiplift chamber structure subsystem can also be derived by using the second type Lagrangian equation.

$$\ddot{Z}_5 + 2\xi_v\sqrt{\frac{\left(K + t_4K\right)}{m_3}}\dot{Z}_5 + \frac{\left(K + t_4K\right)}{m_3}Z_5 - \frac{KR}{m_3}\varphi_1 +$$
$$+\frac{\left(\frac{Ka}{2} - \frac{t_4Ka}{2}\right)}{m_3}\alpha - \frac{t_4KR}{m_3}\varphi_2 + \frac{t_4K}{m_3}z_{22} = 0, \qquad (14)$$

$$\ddot{\alpha} + 2\xi_p\sqrt{\frac{\left(\frac{t_4Ka^2}{4} + \frac{Ka^2}{4}\right)}{J_3}}\dot{\alpha} + \frac{\left(\frac{t_4Ka^2}{4} + \frac{Ka^2}{4}\right)}{J_3}\alpha -$$
$$-\frac{KRa}{2J_3}\varphi_1 + \frac{t_4KRa}{2J_3}\varphi_2 - \frac{t_4Ka}{2J_3}z_{22} +$$
$$+\frac{\left(\frac{Ka}{2} - \frac{t_4Ka}{2}\right)}{J_3}Z_5 = \frac{M}{J_3}. \qquad (15)$$

1.5 Eigen-analysis of MHSF Coupling System

With the MHSF coupling system, it is rather difficult to judge the stability by directly solving the time domain signal. The state-space method is adopted to form a core twenty-one order state matrix. Substituting Eq. (2) into Eq. (15), the Eq. (1), Eq. (5) and Eq. (8) to Eq. (15) can be further organized as follows:

$$\ddot{\alpha} + C_{1,1}\dot{\alpha} + C_{1,2}\alpha - C_{1,3}\varphi_1 + C_{1,4}\varphi_2 - C_{1,5}z_{22} +$$
$$+C_{1,6}Z_5 + C_{1,7}\dot{\beta}_1 + C_{1,8}\beta_1 = 0, \qquad (16a)$$

$$\ddot{\varphi}_1 + C_{2,1}\dot{\varphi}_1 + C_{2,2}\varphi_1 - C_{2,3}Z_5 - C_{2,4}\alpha + C_{2,5}Z_1 +$$
$$+C_{2,6}Z_2 - C_{2,7}\varphi_2 = 0, \qquad (16b)$$

$$\ddot{\varphi}_2 + C_{3,1}\dot{\varphi}_2 + C_{3,2}\varphi_2 - C_{3,3}z_{22} - C_{3,4}Z_5 + C_{3,5}\alpha +$$
$$+ C_{3,6}Z_3 + C_{3,7}Z_4 - C_{3,8}\varphi_1 = 0, \qquad (16c)$$

$$\ddot{Z}_1 + C_{4,1}\dot{Z}_1 + C_{4,2}Z_1 + C_{4,3}\varphi_1 = 0, \qquad (16d)$$

$$\ddot{Z}_2 + C_{5,1}\dot{Z}_2 + C_{5,2}Z_2 + C_{5,3}\varphi_1 = 0, \qquad (16e)$$

$$\ddot{Z}_3 + C_{6,1}\dot{Z}_3 + C_{6,2}Z_3 + C_{6,3}\varphi_2 = 0, \qquad (16f)$$

$$\ddot{Z}_4 + C_{7,1}\dot{Z}_4 + C_{7,2}Z_4 + C_{7,3}\varphi_2 = 0, \qquad (16\,g)$$

$$\ddot{Z}_5 + C_{8,1}\dot{Z}_5 + C_{8,2}Z_5 - C_{8,3}\varphi_1 + C_{8,4}\alpha - C_{8,5}\varphi_2 +$$
$$+ C_{8,6}z_{22} = 0, \qquad (16h)$$

$$\ddot{\beta}_1 + C_{9,1}\dot{\beta}_1 + C_{9,2}\beta_1 + C_{9,3}\alpha + C_{9,4}\dot{\alpha} - C_{9,5}\varphi_1 +$$
$$+ C_{9,6}\varphi_2 - C_{9,7}z_{22} + C_{9,8}Z_5 = 0, \qquad (16i)$$

$$\ddot{z}_{22} + C_{10,1}\ddot{z}_{22} + C_{10,2}\dot{z}_{22} + C_{10,3}z_{22} - C_{10,4}\alpha = 0, \qquad (16j)$$

here $C_{i,j}$ correspond to coefficient terms in Eq. (15), Eq. (8) to Eq. (14), Eq. (1) and Eq. (5). In order to judge the pitch stability, the Eq. (16a) to (16i) should be reduced to first-order. The state vectors are selected as: $x_1 = \dot{\varphi}_1$, $x_2 = \varphi_1$, $x_3 = \dot{\varphi}_2$, $x_4 = \varphi_2$, $x_5 = \dot{\alpha}$, $x_6 = \alpha$, $x_7 = \dot{Z}_1$, $x_8 = Z_1$, $x_9 = \dot{Z}_2$, $x_{10} = Z_2$, $x_{11} = \dot{Z}_3$, $x_{12} = Z_3$, $x_{13} = \dot{Z}_3$, $x_{14} = Z_4$, $x_{15} = \dot{Z}_5$, $x_{16} = Z_5$, $x_{17} = \dot{\beta}_1$, $x_{18} = \beta_1$, $x_{19} = \ddot{z}_{22}$, $x_{20} = \dot{z}_{22}$ and $x_{21} = z_{22}$.

$$\mathbf{x}^{\mathrm{T}} = \begin{bmatrix} x_1 \\ \vdots \\ x_{21} \end{bmatrix}^{\mathrm{T}}. \qquad (17)$$

Combining Eq. (17) and Eq. (16a) to (16i), the state equations of the coupling system can be described by:

$$\frac{d\mathbf{x}}{dt} = \begin{bmatrix} \dot{x}_1 \\ \vdots \\ \dot{x}_{21} \end{bmatrix} = \mathbf{A} \begin{bmatrix} x_1 \\ \vdots \\ x_{21} \end{bmatrix} = \mathbf{Ax}. \qquad (18)$$

This is the central concept of this paper because the pitch stability can be analysed by investigating the eigenvalues of $\mathbf{A}$. The eigenvalue equation of matrix $\mathbf{A}$ can be derived as follows:

$$\sum_{i=0}^{21} b_i \lambda^{21-i} = 0. \qquad (19)$$

Solutions of Eq. (19) are $\lambda_i = \mathrm{Re}_i + \mathrm{Im}_i j$ ($i = 0, 1, ..., 21$), which are not only the eigenvalues of matrix $\mathbf{A}$ but also the main indicators of pitch stability. According to the Lyapunov motion stability theory, the necessary and sufficient condition for the zero-solution stability of a linear system with constant coefficients is that the real parts of all eigenvalues are negative ($\mathrm{Re}_i < 0$).

Since the eigenvalues λ_i are not needed to be expressed analytically, numerical calculation with Mathematica software can be adopted to judge the pitch stability. The algorithm flow is shown as:
(1) For a particular shiplift, substituting structural parameters except a into matrix $\mathbf{A}$, and let $a = 0.01i'$ ($i' = 0, 1, 2, ...$).
(2) For each starting from 0, substituting into the matrix $\mathbf{A}$ to find its eigenvalues. If all the eigenvalues have a negative real part, stopping the cycle and output the critical value of $a = a_{cd}$, where output a_{cd} is the critical distance of suspension points under hydraulic dynamic levelling, which is a key evaluation indicator of the pitch stability. Otherwise, the loop continues until a_{cd} is found.

2 RESULTS AND DISCUSSION

2.1 Validation

In order to illustrate the rationality of the presented model and calculation method, four typical high-lift hoist vertical shiplifts are adopted to be analysed, as shown in Table 1, where a_{cs} is calculated by [6], $n_d = a/a_{cd}$ and $n_s = a/a_{cs}$. The decrease of a_{cd} and a_{cs} indicates pitch stability improvement.

Comparing the a_{cd} and a_{cs} in Table 1, it can be seen that the dynamic hydraulic levelling is enabled to significantly reduce the pitch stability (from 15 % to 44 %). The main reason is that the hydraulic levelling subsystem is coupled in series to the original mechanical-structural-fluid system, reducing the system's overall stiffness. The calculated a_{cd} is the key parameter that has long limited application of hydraulic dynamic levelling in shiplift technical practice.

Table 1. *The distance of suspension points for four typical high-lift hoist vertical shiplifts*

Shiplift name	h [m]	Current status	a_d [m]	a_{cd} [m]	a_{cs} [m]	n_d	n_s	$(n_s - n_d)/n_s$ [%]
GeHeyan shiplift (the first step)	40	In use	23.6	13	8.6	1.8	2.7	34
GeHeyan shiplift (the second step)	82	In use	24.0	19.6	11.6	1.2	2.1	41
GouPitan shiplift (the second step)	127	In use	36.2	33.3	18.5	1.1	2.0	44
200 m level vertical shiplift	200	Design stage	62	56.4	47.9	1.1	1.3	15

Analysing a_d and a_{cd} in Table 1, a_d can guarantee that the shiplift is in stable working condition under hydraulic dynamic leveling. Especially for the 200 m level shiplift, the design parameters can ensure that even if the hydraulic levelling subsystem is started at the most dangerous position, the shiplift chamber is still stable with $n_d = 1.1$.

2.2 Subsystem Stability Priority

In order to study the subsystem stability priority under hydraulic dynamic levelling, the vibration frequency change of each subsystem in the process of gradually reducing a is explored by taking the 200 m level shiplift as an engineering example.

Table 2. *Eigenvalues of 200 m level shiplift coupling system under different distance of suspension points*

Subsystem	Distance of suspension points		
	62	56.4	13
Hydraulic levelling	$-5.33 \pm 161.80j$	$-5.33 \pm 161.80j$	$-5.33 \pm 161.80j$
Hoists	$-3.99 \pm 46.60j$	$-3.99 \pm 46.59j$	$-4.00 \pm 46.56j$
	$-3.93 \pm 44.59j$	$-3.93 \pm 44.59j$	$-3.93 \pm 44.59j$
Suspended wire ropes	$-0.17 \pm 16.24j$	$-0.17 \pm 16.24j$	$-0.17 \pm 16.24j$
	$-0.17 \pm 16.23j$	$-0.17 \pm 16.23j$	$-0.17 \pm 16.23j$
	$-0.47 \pm 9.25j$	$-0.46 \pm 8.93j$	$-0.51 \pm 7.93j$
	$-0.38 \pm 7.56j$	$-0.38 \pm 7.56j$	$-0.38 \pm 7.56j$
Chamber pitch motion	$-0.58 \pm 5.32j$	$-0.54 \pm 4.98j$	$-0.47 \pm 0.34j$
Chamber vertical motion	$-0.23 \pm 3.39j$	$-0.23 \pm 3.39j$	$-0.23 \pm 3.39j$
Shallow water sloshing	$-1.33 \times 10^{-5} \pm 0.22j$	$-8.18 \times 10^{-5} \pm 0.22j$	$0.33 \pm 0.37j$

Here, j is an imaginary number. The negative real part of eigenvalue indicates that the subsystem is stable, otherwise unstable. The larger the absolute value of the real part, the higher the stability and instability margin. The absolute value of the imaginary part represents the vibration frequency of the subsystem [25].

In the process of reducing a from 62 m (design value) to 56.4 m (stable critical value), the eigenvalue real parts of each subsystem are negative, and the shiplift system is in stable state. However, the obvious change is that stability margin of the shallow water sloshing subsystem decreases rapidly (from -1.33×10^{-5} to -8.18×10^{-8}). This means that the shallow water sloshing subsystem is the most vulnerable to instability.

When a is lower than 56.4 m, the eigenvalue real part of the shallow water sloshing subsystem changes from negative to positive, entering the unstable state. Continuing to reduce a to 13 m, causes the eigenvalue real part to become larger (from -8.18×10^{-8} to 0.33), and the unstable vibration of shallow water sloshing subsystem becomes more serious. Meanwhile, the vibration frequency of shiplift chamber structure subsystem is rapidly decreased (from 4.98 rad/s to 0.34 rad/s), close to the unstable vibration frequency of the shallow water sloshing subsystem (from 0.22 rad/s to 0.37 rad/s). The vibration frequencies of the two subsystems are close to the resonance state. It can be inferred that the most unstable one (other than shallow water sloshing subsystem) is the shiplift chamber structure subsystem.

While a is reduced from 56.4 m to 13 m, the vibration frequencies of the hydraulic levelling subsystem and the main hoist subsystem remain stable, and the eigenvalue real part of the hydraulic levelling subsystem (-5.33) is farther away from the virtual axis than the main hoist subsystem (-4.00 to -0.38). The stability margin of the hydraulic levelling subsystem is greater than the main hoist subsystem. For the 200 m level shiplift, the stability priority from high to low is hydraulic levelling subsystem, the main hoist subsystem, the shiplift chamber structure subsystem, and the shallow water sloshing subsystem.

2.3 Influence of Lift Height

Taking the 200 m level shiplift ($a = 62$ m) under hydraulic dynamic levelling as an example, variations of a_{cd} and subsystem vibration frequencies with lift height are analysed in Fig. 4.

It can be seen from Fig. 4a that with the increase of lift height (0 m to 200 m), a_{cd} becomes smaller (56.4 m to 41.2 m), which means that pitch stability is gradually enhanced. The main reason is that the length of suspended wire ropes becomes shorter with the rise of lift height; thus, the stiffness of suspended wire ropes increases rapidly, and pitch stability is enhanced. Figs. 4b to 4f show that the vibration frequencies of hydraulic levelling subsystem, main hoist subsystem, shiplift chamber subsystem, and shallow water sloshing subsystem change stably in their respective regions. For the 200 m level shiplift, pitch stability under dynamic hydraulic levelling can be guaranteed in the whole operation process.
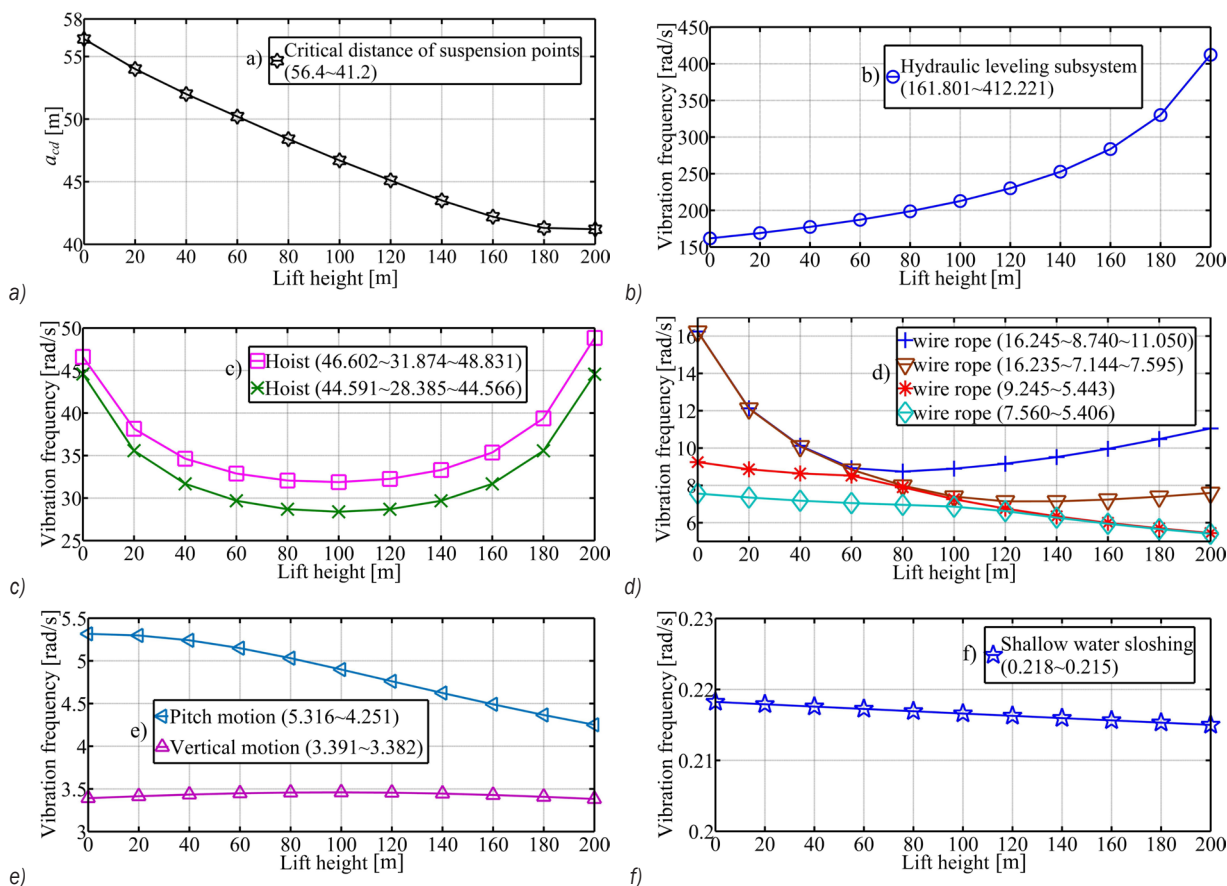
Fig. 4. *Variations of a) critical distance of suspension points, b) hydraulic levelling subsystem vibration frequency,*
c) hoists vibration frequencies, d) wire ropes vibration frequencies,
e) pitch and vertical motion vibration frequencies, f) shallow water sloshing vibration frequency with lift height

2.4 Influence of Synchronous Shaft Stiffness

The synchronous shaft system ensures the synchronization between the hoists and guarantees the shiplift smooth operation. Table 3 shows the variation of a_{cs} and a_{cd} with synchronous shaft stiffness increases.

Table 3. *Effect of synchronous shaft stiffness on the pitch stability of the 200 m level shiplift*

Critical distance of suspension points	Synchronous shaft stiffness increment						
	Design value	5 %	10 %	15 %	20 %	25 %	30 %
a_{cd} [m]	56.4	55.7	55.0	54.4	53.8	53.3	52.9
a_{cs} [m]	47.9	47.2	46.6	46.1	45.5	45.1	44.7

Table 3 displays that the pitch stability is enhanced with the synchronous shaft stiffness increases, regardless of hydraulic dynamic or static levelling. For the hydraulic static levelling, the pitch stability is enhanced by 6.7 % when the synchronous shaft stiffness is increased by 30 %. For the dynamic hydraulic levelling, while the synchronous shaft stiffness raises by 30 %, pitch stability enhances about 6.2 %. It can be inferred that pitch stability of 200 m level shiplift can be effectively improved by increasing the synchronous shaft stiffness, whether it is hydraulic static or dynamic levelling.

2.5 Influence of Damping Ratio

The essence of stability is that system energy decays over time, and finally reaches a state of equilibrium with minimum energy. The subsystem damping plays an essential role in energy dissipation and attenuation. Table 4 analyses the influence of the subsystem damping ratio on the pitch stability.

Table 4. *Effect of subsystem damping ratio on the pitch stability of the 200 m level shiplift*

Series	ξ_j	ξ_g	ξ_v	ξ_p	ξ_w	ξ_h	a_{cd} [m]
1	0.1	0.01	0.005	0.05	0.00024	0.03	56.4
2	0.1	0.01	0.005	0.05	2×0.00024	0.03	44.8
3	0.1	0.01	0.005	0.05	0.00024	2×0.03	56.39

where ξ_g refers to [2], ξ_j and ξ_j are adopted from [4], ξ_v comes from [6], ξ_w is calculated according to [26] and ξ_h is obtained by Eq. (3c).

Comparing series 1 and series 2, when ξ_w is doubled, pitch stability safety factor is raised from 1.1 (i.e. 62 / 56.4) to 1.4 (i.e. 62 / 44.8). That is, increasing ξ_w can effectively improve the pitch stability. The main reason is that the weakest stability link in the MHSF coupling system is the shallow water sloshing subsystem, and the increase of the sloshing damping ratio can accelerate the convergence and enhance stability. When the shiplift works, because of the existence of ship in the chamber, ξ_w is greatly increased, and sloshing is suppressed. Compared with the ship-free state, pitch stability is improved, and the safety factor in the actual operation process is higher than the calculated value 1.1.

Comparing series 1 and series 3, while ξ_h is doubled, a_{cd} is essentially unchanged. That is, ξ_h hardly affects the pitch stability. The main reason is that the hydraulic levelling subsystem has the highest stability priority in the coupling system. Increasing is equivalent to raise the upper limit of stability but does not affect the lower limit of stability.

3 CONCLUSIONS

A new MHSF coupling dynamics model and a developed semi-analytical method are presented to investigate the pitch stability under hydraulic dynamic levelling. Taking four typical high-lift hoist vertical shiplifts as examples, the reliability of the proposed model and method is illustrated. The subsystem stability priority and influence factors on the pitch stability are analysed in detail. Pitch stability of the 200 m level shiplift under dynamic hydraulic levelling is focused. The key observations are summarized as follows:

1. Based on the closed-loop transfer function, multi-modal theory and second type Lagrangian equation, the models of hydraulic levelling subsystem, shallow water sloshing subsystem, the main hoist mechanical subsystem and shiplift chamber structure subsystem are built, respectively. Subsequently, a core 21 order state matrix of the MHSF coupling system is proposed using state-space method.

2. A developed semi-analytical method integrating the Lyapunov motion stability theory and the Eigen-analysis method is proposed to judge the pitch stability and analyse subsystem characteristics. The results indicate that pitch stability under dynamic hydraulic levelling is reduced by 15 % to 44 % with respect to hydraulic static levelling, but dynamic hydraulic levelling will not cause instability. For the designed 200 m level shiplift, the critical distance of suspension points is 56.4 m, and the design parameters can guarantee the pitch stability safety factor under dynamic hydraulic levelling not less than 1.1.

3. In the MHSF coupling system, the stability priority from high to low is the hydraulic levelling subsystem, the main hoist subsystem, shiplift chamber structure subsystem, and the shallow water sloshing subsystem.

4. For the designed 200 m level shiplift, pitch stability enhances significantly (maximum 26.98 %) as the lift height increases (0 m to 200 m). Improving the synchronous shaft stiffness by 30 % can enhance the pitch stability about 6.2 %. Doubling the water boundary layer damping ratio can raise the pitch stability about 20.57 %.

4 ACKNOWLEDGMENTS

5 NOMENCLATURES

a distance of suspension points, [m]
a_d distance of suspension points given by designers, [m]
a_{cd} critical distance of suspension points under hydraulic dynamic levelling, [m]
a_{cs} critical distance of suspension points under hydraulic static levelling, [m]
A state matrix of MHSF coupling system
A_1 non-rod cavity area of hydraulic cylinder, [m²]
A_2 rod cavity area of hydraulic cylinder, [m²]
b_i eigenvalue equation coefficients
B width of shiplift chamber, [m]
B_1 hoist at upstream
B_2 pulley at upstream
B_3 pulley at downstream
B_4 hoist at downstream

c center point of shiplift chamber bottom

C equivalent synchronous shaft stiffness, [N·m·rad^{-1}]

$C_{i,j}$ coefficient expressions

C_t total leakage coefficient related to load pressure, [m^5·N^{-1}·s^{-1}]

g gravity acceleration, [m·s^{-2}]

$G(s)$ transfer function of valve controlled asymmetric hydraulic cylinder

$G_B(s)$ closed-loop transfer function

h lift height, [m]

H water depth of shiplift chamber, [m]

J_1 equivalent inertia moment of hoist, [kg·m^2]

J_2 equivalent inertia moment of pulley, [kg·m^2]

J_3 equivalent inertia moment of shiplift chamber, [kg·m^2]

k equivalent load wire rope stiffness, [N·m^{-1}]

K equivalent stiffness of wire ropes at upstream, [N·m^{-1}]

K_a proportional amplifier gain

K_{sv} flow gain of proportional speed regulating valve

K_f sensor gain

K_q flow gain

K_{ce} total pressure flow coefficient including leakage, [m^5·N^{-1}·s^{-1}]

K_c pressure-flow factor (the change rate of the load flow rate relative to the load pressure when the valve spool displacement is constant), [m^5·N^{-1}·s^{-1}]

L length of shiplift chamber, [m]

m_1 half weight of torque counterweight, [kg]

m_2 half weight of gravity counterweight, [kg]

m_3 total weight of shiplift chamber, [kg]

M hydrodynamic moment with respect to point c, [N·m]

M_t equivalent mass of piston and load wire rope, [kg]

n effective area ratio of two cavities of hydraulic cylinder

n_d pitch stability safety factor under hydraulic dynamic levelling

n_s pitch stability safety factor under hydraulic static levelling

R radius of hoists and pulleys, [m]

t_1 torsional stiffness ratio of synchronous shaft and motor drive shaft

t_2 influence factor on torque counterweight suspended wire rope at upstream

t_3 influence factor on gravity counterweight suspended wire rope at upstream

t_4 influence factor of elasticity modulus tolerance

t_5 influence factor on gravity counterweight suspended wire rope at downstream

t_6 influence factor on torque counterweight suspended wire rope at downstream

T kinetic energy, [J]

V potential energy, [J]

V_t total volume of two cavities of hydraulic cylinder, [m^3]

$\mathbf{x}$ state vector matrix

z_{22} piston displacement, [m]

Z_1 torque counterweight vertical displacement at upstream, [m]

Z_2 gravity counterweight vertical displacement at upstream, [m]

Z_3 gravity counterweight vertical displacement at downstream, [m]

Z_4 torque counterweight vertical displacement at downstream, [m]

Z_5 shiplift chamber vertical displacement, [m]

α pitch angular displacement, [rad]

β_1 first order modal function of sloshing

β_e elastic modulus of oil, [Pa]

ξ_w first order water boundary-layer damping ratio

ξ_h hydraulic damping ratio

ξ_j torsional vibration damping ratio

ξ_g wire rope damping ratio

ξ_p pitch motion damping ratio

ξ_v vertical motion damping ratio

Σ_0 mean free surface

ρ water density, [kg·m^{-3}]

φ_1 rotating angle displacement of hoist and pulley at upstream, [rad]

φ_2 rotating angle displacement of hoist and pulley at downstream, [rad]

ω_1 first order natural frequency of fluid in the shiplift chamber, [rad·s^{-1}]

ω_h hydraulic natural frequency, [rad·s^{-1}]

ω_r turning frequency of inertial link, [rad·s^{-1}]

6 REFERENCES

[1] Yu, Q., Fang, X. (2008). Application of hydraulic pressure technology in modern shiplift. *Yangtze River*, vol. 39, no. 20, p. 71-72, **DOI:10.3969/j.issn.1001-4179.2008.20.026**. (in Chinese)

[2] GB 51177(2016). *Design Code for Shiplift*. The Ministry of Water Resources of the People's Republic of China. Beijing, China. (in Chinese)

[3] Cheng, G., Li, H., Ruan, S. (2005). Free vibration characteristics and stability analysis of shiplift system. *Journal of Mechanical Strength*, vol. 27, no. 3, p. 276-281, **DOI:10.3321/j.issn:1001-9669.2005.03.002**. (in Chinese)

[4] Liao, L. (2014). Safety analysis and design of full balanced hoist vertical shiplifts. *Structural Engineering and Mechanics*, vol. 49, no. 3, p. 311-327, **DOI:10.12989/sem.2014.49.3.311**.

[5] Cheng, X., Shi, D., Li, H., Xia, R., Zhang, Y., Zhou, J. (2018). Stability and parameters influence study of Fully Balanced Hoist Vertical Ship Lift. *Structural Engineering and Mechanics*, vol. 66, p. 583-594, **DOI:10.12989/sem.2018.66.5.583**.

[6] Zhang, Y., Shi, D., Liao, L., Shi, L., Cheng, X. (2019). Pitch stability analysis of high-lift wire rope hoist vertical shiplift under shallow water sloshing–structure interaction. *Proceedings of the Institution of Mechanical Engineers, Part K: Journal of Multi-Body Dynamics*, **DOI:10.1177/1464419319850666**.

[7] Niu, W., Wang, S., Wang, Y., Song, Y., Zhu, Y. (2017). Stability analysis of hybrid-driven underwater glider. China Ocean Engineering, vol. 31, no. 5, p. 528-538, **DOI:10.1007/s13344-017-0061-y**.

[8] Banshchikov, A., Bourlakova, L. (2001). Computer algebra and problems of motion stability. *Mathematics and Computers in Simulation*, vol. 57, no. 3-5, p. 161-174, **DOI:10.1016/s0378-4754(01)00336-6**.

[9] Ahmad, S., Yue, B. (2012). Motion stability dynamics for spacecraft coupled with partially filled liquid container. *Theoretical and Applied Mechanics Letters*, vol. 2, no. 1, art. ID 013002, **DOI:10.1063/2.1201302**.

[10] Wu, Q., Zhang, L., Ma, Z. (2017). A model establishment and numerical simulation of dynamic coupled hydraulic–mechanical–electric–structural system for hydropower station. *Nonlinear Dynamics*, vol. 87, p. 459–474, **DOI:10.1007/s11071-016-3053-1**.

[11] Peng, H., Pan, E., Zhong, T., Hu, Z. (2004). Analysis on tension balance characteristic of hydraulics system of three gorges shiplift. *Chinese Journal of Mechanical Engineering*, vol. 40, no. 1, p. 155-159, **DOI:10.3321/j.issn:0577-6686.2004.01.031**. (in Chinese)

[12] Zeng, W., Yang, J., Yang, W. (2016). Instability analysis of pumped-storage stations under no-load conditions using a parameter-varying model. *Renewable Energy*, vol. 90, p. 420-429, **DOI:10.1016/j.renene.2016.01.024**.

[13] Zheng, Y., Eben Li, S., Wang, J., Cao, D., Li, K. (2015). Stability and scalability of homogeneous vehicular platoon: study on the influence of information flow topologies. *IEEE Transactions on Intelligent Transportation Systems*, p. 1-13, **DOI:10.1109/TITS.2015.2402153**.

[14] Martynyuk, A. (2003). *Advances in Stability Theory at the End of the 20th Century*. CRC Press, London, **DOI:10.1201/b12543**.

[15] Stojanović, V., Petković, M., Deng, J. (2018). Instability of vehicle systems moving along an infinite beam on a viscoelastic foundation. *European Journal of Mechanics AsSolids*, vol. 69, p. 238-254, **DOI:10.1016/j.euromechsol.2017.12.007**.

[16] Liu, X., Liu, C. (2007). Eigenanalysis of oscillatory instability of a hydropower plant including water conduit dynamics. *IEEE Transactions on Power Systems*, vol. 22, no. 2, p. 675-681, **DOI:10.1109/TPWRS.2007.895156**.

[17] Yang, W., Norrlund, P., Chung, C., Yang, J., Lundin, U. (2018). Eigen-analysis of hydraulic-mechanical-electrical coupling mechanism for small signal stability of hydropower plant. *Renewable Energy*, vol. 115, p. 1014-1025, **DOI:10.1016/j.renene.2017.08.005**.

[18] Yu, X., Zhang, J., Fan, C., Chen, S. (2016). Stability analysis of governor-turbine-hydraulic system by state space method and graph theory. *Energy*, vol. 114, p. 613-622, **DOI:10.1016/j.energy.2016.07.164**.

[19] Yu, X.D., Zhang, J., Chen, S., Liu, J.C. (2016). Stability analysis of the governor-turbine-hydraulic system of pumped storage plant during small load variation. *IOP Conference Series: Earth and Environmental Science*, vol. 49, art. ID 112004, **DOI:10.1088/1755-1315/49/11/112004**.

[20] Zhang, Y., Shi, D., Shi, L., Xia, R., Cheng, X., Zhou, J. (2019). Analytical solution of capsizing moments in ship chamber under pitching excitation. *Proceedings of the Institution of Mechanical Engineers, Part C: Journal of Mechanical Engineering Science*, vol. 233, no. 15, p. 5294-5301, **DOI:10.1177/0954406219843327**.

[21] Shi, L., Zhang, Y., Cheng, X.H., Zhou, J., Shi, D.W., Xia, R. (2019) Stability analysis of Hoist Vertical Shiplift chamber under pitching motion. *IOP Conference Series: Materials Science and Engineering*, vol. 631, art. ID 032028, **DOI:10.1088/1757-899X/631/3/032028**.

[22] Stephen, J.J., Sannasiraj, S.A., Sundar, V. (2016). Numerical simulation of sloshing in a rectangular tank under combined horizontal, vertical and rotational oscillations. *Proceedings of the Institution of Mechanical Engineers. Part M: Journal of Engineering for the Maritime Environment*, vol. 230, no. 1, p. 95-113, **DOI:10.1177/1475090214533512**.

[23] Faltinsen, O.M., Timokha, A.N. (2009). *Sloshing*. Cambridge University Press, Cambridge.

[24] Walters R.B. (2000) System Analysis of Electro-hydraulic Control Systems. In: *Hydraulic and Electric-Hydraulic Control Systems*. Springer, Dordrecht, **DOI:10.1007/978-94-015-9427-1_12**.

[25] Blair, T. H. (2016). Control Systems. *Energy Production Systems Engineering*. John Wiley and Sons, Inc. **DOI:10.1002/9781119238041.ch23**.

[26] Keulegan, G. (1959). Energy dissipation in standing waves in rectangular basins. *Journal of Fluid Mechanics*, vol. 6, no. 1, p. 33-50, **DOI: 10.1017/S0022112059000489**.